Catalysis Communications 76 (2016) 23–28

Contents lists available at ScienceDirect

Catalysis Communications

journal homepage: www.elsevier.com/locate/catcom

Short Communication

Electrodeposited Re-promoted Ni foams as a catalyst for the dry reforming of methane

Brian A. Rosen [a,*], Eliezer Gileadi [b], Noam Eliaz [a]

[a] Department of Materials Science and Engineering, Faculty of Engineering, Tel Aviv University, Ramat Aviv 69978001, Israel
[b] School of Chemistry, Faculty of Exact Sciences, Tel Aviv University, Ramat Aviv 69978001, Israel

ARTICLE INFO

Article history:
Received 11 October 2015
Received in revised form 2 December 2015
Accepted 15 December 2015
Available online 17 December 2015

Keywords:
Methane reforming
Electrodeposition
Metal foams

ABSTRACT

The dry reforming of methane (DRM) utilizes carbon dioxide (CO_2) as the oxidizing agent in order to produce synthesis gas. Catalyst deactivation via coking, oxidation, and sintering has stymied the industrialization of catalysts for the DRM. Here, we utilized electrodeposition followed by de-alloying in order to synthesize metal alloy foams (5 m^2/g). Through this process we have created the first electrodeposited DRM catalyst capable of converting more than 10,000 mL/g∗h at near-equilibrium conversion. Rhenium promotion was observed over the entire temperature range studied (700–800 °C), with the most dramatic enhancement at 700 °C. After 50 h of reaction, no significant accumulation of carbonaceous deposits were detected, making electrodeposited structures a viable candidate for stable methane conversion catalysts.

1. Introduction

Significant attention has been given over the last 20 years towards the dry reforming of methane (DRM). Typically, methane is reformed with steam as the oxidizing agent (Eq. (1)); however, such high H_2:CO ratios are undesirable for downstream processing into long-chain hydrocarbons such as synthetic liquid fuels via Fischer–Tropsch synthesis [1]. The DRM (Eq. (2)) utilizes carbon dioxide (CO_2) as the oxidizing agent in order to decrease the H_2:CO ratio from 3:1 to 1:1 as shown below.

$$CH_4 + H_2O \leftrightarrow 3H_2 + CO \tag{1}$$

$$CH_4 + CO_2 \leftrightarrow 2H_2 + 2CO \tag{2}$$

The primary factor preventing the industrialization of the DRM is the lack of catalyst materials resistant to deactivation [2]. In the case of supported catalyst, deactivation primarily occurs through carbon deposition [3], oxidation [4], or sintering of active sites [5]. Therefore, DRM catalyst materials resistant to these forms of deactivation are highly desirable.

The vast majority of DRM studies focus their attention on supported catalysts where active metallic phases (typically, alloys of noble metals with Ni, Fe, and/or Co) are distributed about metal-oxide nanoparticles [6]. While such materials have the advantage of providing large surface areas (BET surface areas typically between 20 and 200 m^2/g), they can exhibit large pressure drops and poor heat transfer compared to conductive structured catalysts. This can be particularly devastating for highly endothermic (including DRM, $\Delta H^0 = +247$ kJ/mol) [2] and exothermic reactions, as temperature gradients will inevitably form. Nevertheless, structured catalysts such as metallic gauzes and foams can be designed to offer a low flow resistance, short diffusion distances, and higher thermal conductivities compared to porous ceramic supports [7]. The design of highly active metallic foam catalysts, such as the materials described in this work, may therefore compromise between the need for specific surface area and effective heat and mass transfer.

Previous efforts to design structured wire catalysts for methane reforming either required the presence of steam at high pressures and temperatures [8] or low gas-hourly space velocities [9] in order to achieve high conversion or stable performance. In this work, we show that low-level rhenium alloying (0.5–1.5 at.%) can lead to high and stable DRM activity at large space velocities at atmospheric pressure. While rhenium is currently used in various fuel reforming applications, only a handful of studies have investigated its capacity to catalyze or promote DRM [10–12]. Despite rhenium's coke-resistant properties, these reports cite the volatility [13] and high operating temperatures [14] as drawbacks for its use. Here, the favorable reducibility of bulk metallic phases (by comparison to nanopowder supported phases which can show low reducibility due to stabilization [15]) is exploited to design a material where rhenium promotion of DRM is stable at lower temperatures. Furthermore, the procedure described here only requires low levels of Re, making our method much more viable for future industrial applications.

2. Experimental

2.1. Catalyst preparation

Stainless steel type 316 gauze (325 mesh woven from 36-μm diameter wires) was provided by Alfa Aesar. The nominal chemical

---

[*] Corresponding author.

http://dx.doi.org/10.1016/j.catcom.2015.12.014
1566-7367/

composition of the wire material was 67.5 wt% Fe, 17 wt% Cr, 13 wt% Ni, and 2.5 wt% Mo, as provided by the manufacturer. The gauze was laser-cut into circular samples (dia 14 mm). The cut samples were cleaned by sonication for 15 min in 32 vol% HCl in DI water. The sonicated samples were rinsed and sonicated for another 15 min in DI water.

2.2. Electrodeposition

The electroplating bath was prepared using 180 mM nickel sulfamate and 180 mM citric acid, and was adjusted to pH 5 ± 0.1 using 5 M sodium hydroxide. Rhenium-alloyed samples were fabricated using the same bath, but with the addition of up to 3 mM ammonium perrhenate. Electrodeposition of pure Ni and Ni–Re alloys onto the stainless steel gauze was done by immersing the gauze sample into the proper electrolyte fixed between two platinum gauze (52 mesh) counter electrodes spaced 1 cm away on either side. Electrodeposition was carried out in a jacketed electrochemical cell with a magnetic stir-bar connected to a heated bath recirculator set to 60 °C. Electrochemical measurement and control was through Princeton Applied Research 263A Potentiostat/Galvanostat. The electrodeposition was galvanostatic at a current density of 40 mA/cm^2 for 800–1100 s, as required to deposit a 10-μm layer (~36 mg).

2.3. Catalyst testing assembly

Catalysts were placed inside a 12-mm ID quartz tube ($L = 60$ mm, OD = 15 mm) in the isothermal zone of an Electrotherm tube furnace. The temperature of the isothermal zone was changed using the integrated controller on the furnace chassis. The temperature of the catalyst was measured using a K-type thermocouple. In order to prevent reaction on the thermocouple surface, we placed the thermocouple on the outside of the tube at the lateral position of the catalyst. A separate experiment utilizing 2 K-type thermocouples was conducted to measure the differential temperature between the catalyst surface and the outer thermocouple. All temperatures reported in this report refer to the temperature of the catalyst. The reaction mixture was created by mixing argon, carbon dioxide, and methane using Alicat mass flow controllers (MFCs). The mixture had a molar CO_2:CH_4:Ar ratio of 1:1:8. Mixing occurred at atmospheric pressure prior to delivery into the furnace. No significant pressure drop was observed across the loaded quartz tube owing to the low flow resistance provided by the foam catalyst. After the furnace, the converted gas was sent through trace-heated (110 °C) tubing to an SRI gas chromatograph fitted with Molecular Sieve 13X and Hysep C columns. The GC contained two thermal conductivity detectors (TCDs) and a methanizer-flame ionization detector (FID). Hydrogen was quantified using a TCD with a nitrogen carrier, CO, CO_2, and CH_4 were quantified using the methanizer-FID, and O_2, N_2 were measured using a TCD with a helium carrier.

2.4. Sample transfer

In order to prepare our samples for ex-situ analysis, the reactor was purged and cooled in an argon environment in order to prevent unwanted oxidation of our catalyst between the reactor and the XRD analysis. Furthermore, samples were stored in a desiccated vacuum chamber. We cannot completely rule out the possibilty of oxidation during the transfer process, however, these processes were present in both the pre- and post-reaction XRD spectra. Furthermore, the most abundant phase of rhenium was completely absent from the pre-reaction XRD spectra. Therefore, despite the reality of oxidation during the transfer process, we find the XRD analysis to give a meaningful and reliable description of our material.

3. Results and discussion

Fig. 1 shows that the coating displays a mesoscale colony surface morphology as is typical of Ni-based electrodeposits at 40 mA/cm^2. Such morphology was observed in Ni and Ni-alloy electrodeposits whenever the applied current density exceeded the mass-transport limiting current density [16].

Elemental mapping of the cross-section of the precursor Ni–Re layer (Fig. 2A) reveals that the Re-content is highest at the interface between the stainless steel substrate and the coating (14 at.%) and lowest at the outer surface (5 at.%) due to the depletion of the perrhenate ion in the electrolyte during electrodeposition. To form the final catalyst material, the Ni–Re- and Ni-coated gauzes were then calcined at 900 °C in a 10^{-1} Torr vacuum for 16 h, during which time the volatile nickel oxide (NiO) and rhenium oxide (Re_2O_7) were partially removed from the coating, transforming the catalyst deposit from a compact layer into a metal foam (BET surface area of 5.1 cm^2/g; pore volume of 0.012 cm^3/g), also shown in Fig. 1. Furthermore, the mass lost in the calcination step was approximately 17%.

Elemental dot maps of the post-reaction catalyst (Fig. 2B) show the outward diffusion of both iron and chromium into the catalyst foam layer. The diffusion of iron into the catalyst foam layer is significant because iron, while not very active for methane reforming, has been shown to prevent the accumulation of carbonaceous deposits [17]. Furthermore, a significant amount of chromium segregated to the stainless steel surface, typical effect found in austenitic stainless steels at elevated temperatures [18]. The level of outward diffusion of iron and chromium into the catalyst layer was not found to be impacted by the presence of Re. The atomic Re-content of the final catalyst material ranged from 1.5 at.% at the stainless steel interface to 0.5 at.% at the outer surface of the foam (from XPS). Cross-sectional analysis also revealed that the porosity of the catalyst layer was greatest adjacent to the steel gauze support and dropped off towards the outer surface. While still containing pores, the catalyst layer near the outer surface was more compact as

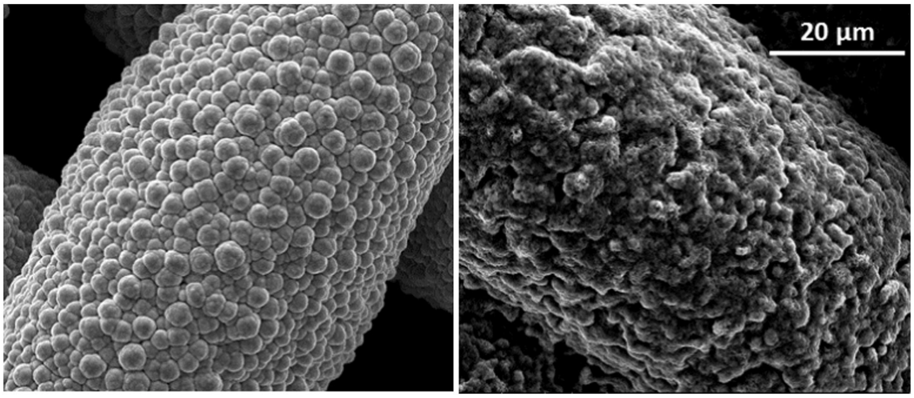

Fig. 1. SEM images of the Ni–Re catalyst precursor surface morphology as-deposited (left) and post-reaction (right). Scale bar shown is for both images.

it was formed as a result of re-deposition during calcination. This is evident by the increased catalyst layer thickness. For simplicity, all references to the composition of the final catalyst material will refer to the composition at the outer surface of the coating.

Re-promoted (Ni–Re/S.S) and Re-free (Ni/S.S) foams were tested for DRM catalytic activity by measuring the single-pass conversion of CH_4 and CO_2 (1:1) diluted in Ar (80 mol%) at atmospheric pressure and temperatures between 700 and 800 °C. Prior to exposure to the reaction gas mixture, the catalysts were reduced in a 10% H_2 in Ar for 2 h at 700 °C [18–19]. The effect of Re alloying was evaluated by comparing the conversion of the Re-alloyed foams with their unalloyed counterpart. Fig. 3A and B show the single-pass conversion of CH_4 and CO_2 over the Ni–Re/S.S and Ni/S.S. catalyst at 700, 750, and 800 °C. All experiments were performed at a gas-hourly space velocity (GHSV) of 16,000 mL/(h·g_{cat}) (at room temperature) where the flow rate of argon was not considered and g_{cat} is the mass of the catalyst. The bare stainless steel gauze showed only minimal catalytic activity (<2% conversion) at this space velocity owing to its extremely low specific surface area. Therefore, the role of the stainless steel gauze is to provide iron and mechanical support to the electrodeposited layer, and does not significantly contribute to the measured conversion.

Fig. 3A and B show that at 750 and 800 °C, the Ni–Re/S.S material performed 10% better than the unalloyed Ni/S.S catalyst, and operated near-equilibrium conversion. The increase in conversion within this temperature range is attributed to ReO_x promotion of the DRM. At 750 and 800 °C, the addition of 0.2% Re had almost no effect on methane

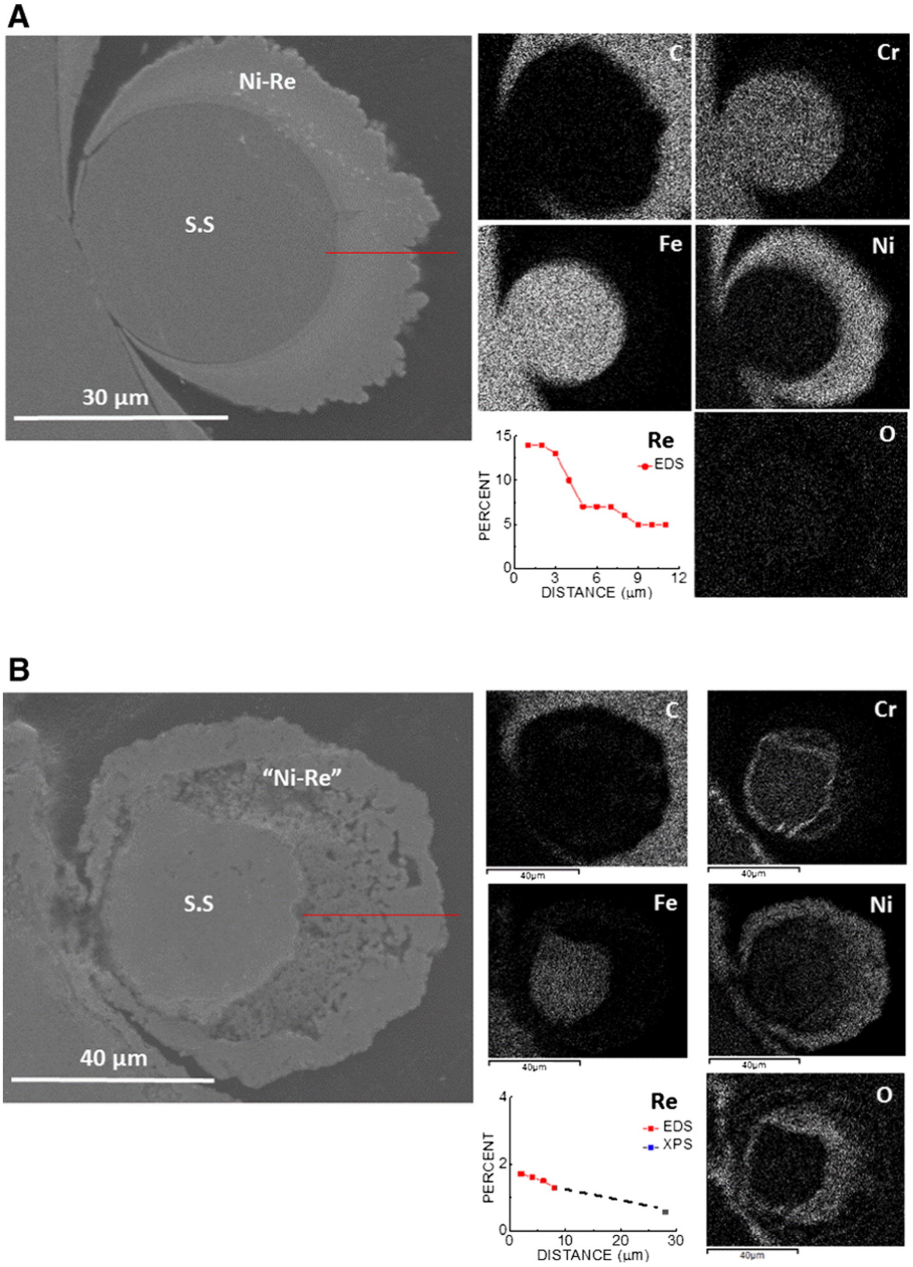

Fig. 2. A: SEM cross-section of an as-deposited Ni–Re coating on a stainless steel (S.S) wire. Elemental dot maps (EDS) are shown for C, Cr, Fe, Ni, and O. Atomic percent Re-content shown as a linescan (EDS). Solid red line in SEM micrograph shows the location of the Re linescan. B: SEM cross-section of the Ni–Re catalyst layer on a stainless steel (S.S) wire post-reaction. Elemental dot maps (EDS) are shown for C, Cr, Fe, Ni, and O. Atomic percent Re-content shown as a linescan (EDS) until a distance of 8 µm away from the stainless steel core, after which point the Re-content fell below EDS sensitivity. Atomic percent Re at outer surface was measured by XPS. Solid red line in SEM micrograph shows the location of the Re linescan. (For interpretation of the references to color in this figure legend, the reader is referred to the web version of this article.)

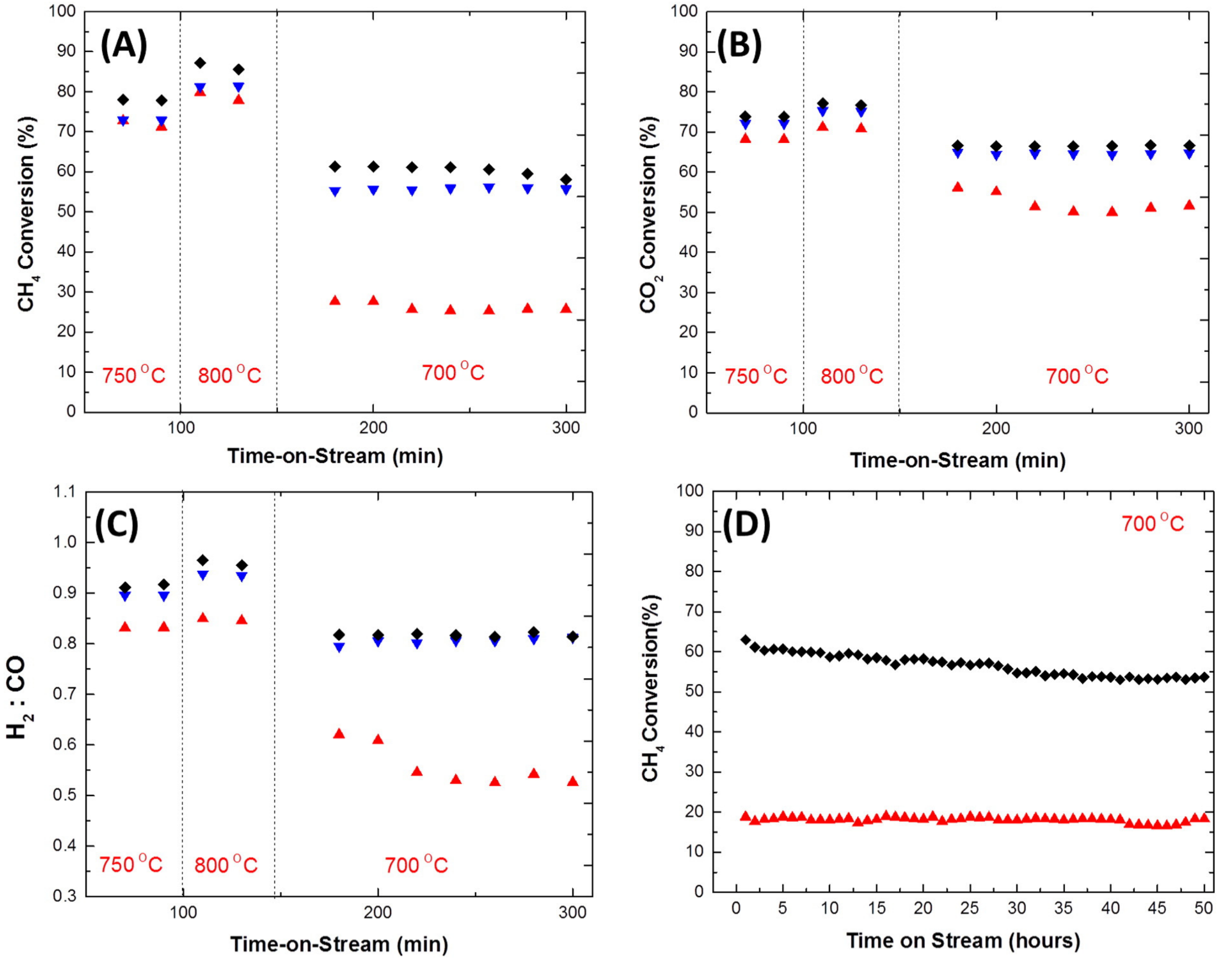

Fig. 3. Single-pass methane (A) and carbon dioxide (B) conversions at various operating temperatures. H_2:CO product ratio shown in (C). Lifetime testing shown in (D). All data points shown are at a GHSV of 16,000 $mL_{gas}/(g_{cat} \cdot h)$ and a CH_4:CO_2 feed ratio of 1:1. (♦) Ni–Re/S.S ($Ni_{93.5}Fe_{6.0}Re_{0.5}$) (▼) $Ni_{93.8}Fe_{6.0}Re_{0.2}$ (▲) Ni/S.S ($Ni_{94.0}Fe_{6.0}$). Under operating conditions, equilibrium conversions of methane at 700, 750, and 800 °C are 91.5%, 94.4%, and 96.3% respectively. Equilibrium conversions for carbon dioxide at the same temperatures are 66.3%, 79.1%, and 88.6%.

conversion. However, when the temperature was decreased to 700 °C, the Re-alloyed (both 0.2 and 0.5% Re) catalysts doubled their conversion of methane compared to the unalloyed material.

We do not attribute the drop in DRM activity for the Ni-only catalysts at 700 °C to carbon formation as coking is a gradual process and generally not the cause of an abrupt change in activity as observed here. Furthermore, TPO/TGA (Figure S1), XRD (Figure S2), and TEM (Figure S3) revealed no signs of accumulated carbon compounds or carbonate species in the spent catalysts. This result is significant as it suggests that the primary form of deactivation is not coke accumulation but rather oxidation or grain growth. The drop in activity here is attributed to Ni oxidation (forming the inactive NiO phase, XPS Fig. 4A) due to the decrease in hydrogen and carbon monoxide production (Fig. 3C), both of which act as in situ reducing agents [20]. Temperature programmed reduction (TPR) of both Ni/S.S. and Ni–Re/S.S. shown in Figure S4 revealed only a small shift in the peak reduction temperature of NiO when such low Re contents were present. However, the hydrogen uptake of the Re-promoted catalyst was much larger compared to the Ni-only catalyst. Re-promotion of DRM at 700 °C is therefore attributed to larger surface H_2 and CO concentrations, which in turn prevents Ni oxidation. Guczi et al. also found that NiO reduced to Ni^0 above 700 °C through the same mechanism, quickly increasing the activity of the catalyst to equilibrium conversion as seen here.

The drop in carbon dioxide conversion over the Re-free catalyst (Fig. 3B) was not nearly as dramatic as observed with methane. This difference is attributed to the reverse water gas shift (RWGS) reaction (Eq. (3)), a common DRM side reaction present under all studied temperatures as it is only slightly endothermic (41 kJ/mol), with an equilibrium constant near unity. [21] Although the DRM is suppressed by Ni oxidation at 700 °C, nickel (II) hydroxide still present on the surface (Fig. 4) is a known catalyst for the RWGS [22], thereby maintaining the conversion of additional CO_2.

$$CO_2 + H_2 \leftrightarrow H_2O + CO \tag{3}$$

To put the activity of our catalyst in perspective, one should note that despite a drop in specific surface area of 30-fold compared to many supported powder catalysts, the Ni–Re foams showed comparable performance (as measured by conversion) at similar space velocities. This material represents the first metal foam (not based on nanoparticle dispersion on a monolith) capable of stable DRM performance at elevated space velocities (>10,000 $mL/(h \cdot g_{cat})$). Furthermore, while rhenium's performance as a DRM catalyst was found to be most active at elevated temperatures (>850 °C) in previous works [14], its effectiveness as a promoter after alloying into the Ni-foam is evident here at lower temperatures.

Results from the stability tests for both Ni–Re/S.S and Ni/S.S catalysts at 700 °C are shown in Fig. 3D. The performance of the Re-alloyed Ni foams more than doubled that of the unalloyed material over the entire 50-h test period, consistent with the temperature programmed study. The initial decrease in conversion for the Ni–Re/S.S sample is likely

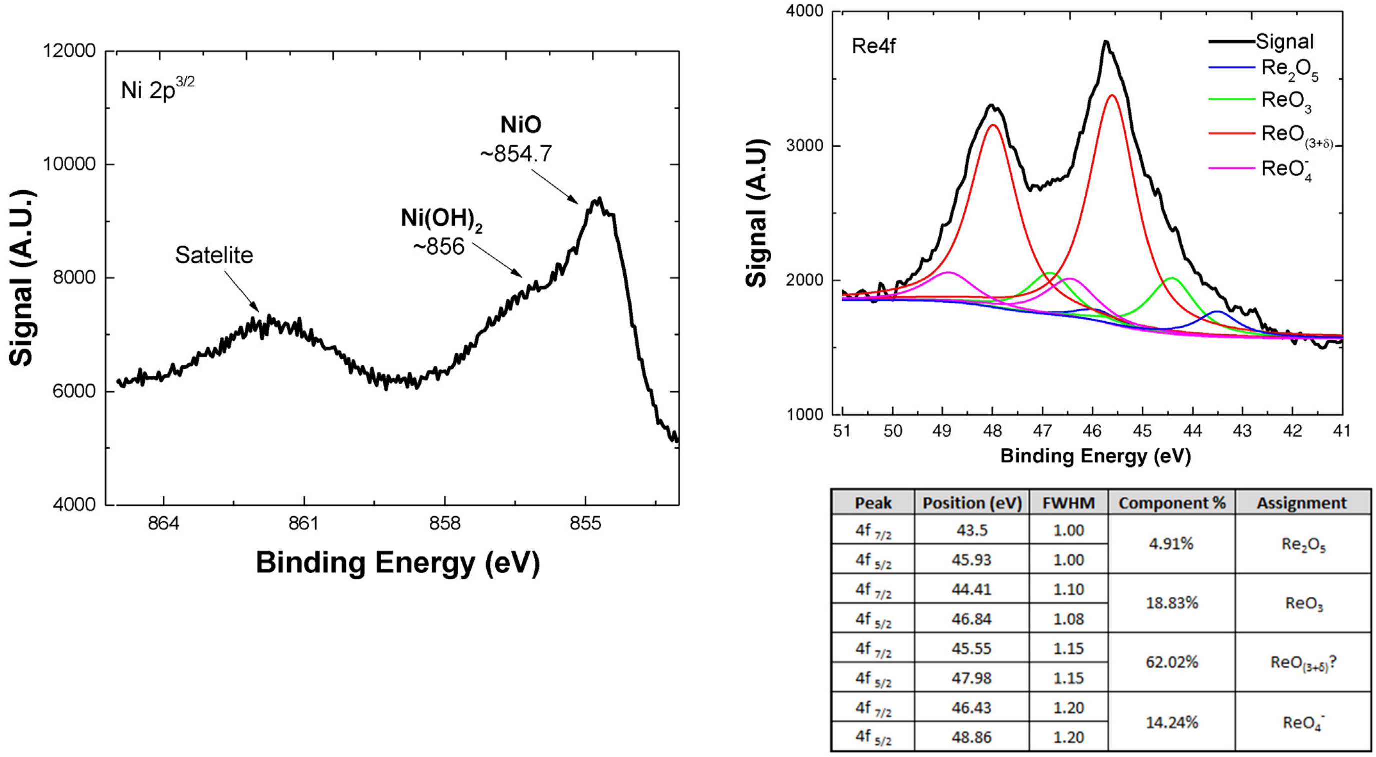

Peak	Position (eV)	FWHM	Component %	Assignment
4f $_{7/2}$	43.5	1.00	4.91%	Re_2O_5
4f $_{5/2}$	45.93	1.00		
4f $_{7/2}$	44.41	1.10	18.83%	ReO_3
4f $_{5/2}$	46.84	1.08		
4f $_{7/2}$	45.55	1.15	62.02%	$ReO_{(3+\delta)}$?
4f $_{5/2}$	47.98	1.15		
4f $_{7/2}$	46.43	1.20	14.24%	ReO_4^-
4f $_{5/2}$	48.86	1.20		

Fig. 4. (Left): X-ray photoelectron spectrum of spent Ni–Re/S.S catalyst showing the $Ni(OH)_2$ and NiO peaks. (Right): Measured (black) and deconvoluted Re4f spectra of spent Ni–Re catalyst with phase assignment and content.

due to the partial oxidation of rhenium in the presence of CO_2 as this initial drop was not present in the unalloyed sample. Ni–Re/S.S catalysts were also tested at various values of the GHSV (Figure S5). As the GHSV was raised above 60,000 $mL/(h \cdot g_{cat})$, the methane conversion dropped linearly, suggesting that the reason for the drop in conversion was due to active-site saturation.

Ex-situ XRD analysis of our samples both before and after reaction gave insight to the species causing both promotion and deactivation. As-deposited Ni–Re coatings typically showed surface rhenium present as Re^0, intermetallic Ni–Re, and Re (IV–VII) oxides. Prior to catalysis, almost 40% of the surface rhenium was present in its fully oxidized +7 state. XPS analysis of the Ni–Re/S.S catalyst after 50 h on-stream (Fig. 4) revealed no metallic or intermetallic rhenium, suggesting that the oxides of rhenium, and not Re^0 or Ni–Re intermetallic compounds, promote DRM.

Deconvolution of the post-reaction Re4f peaks revealed a majority of the Re signal came from $4f_{7/2}$ and $4f_{5/2}$ peaks centered at 45.55 eV and 47.98 eV, respectively. These binding energies do not match any of the oxidation states of common Re-oxides and imply that the effective oxidation state of Re within this oxide phase is a non-integer value between +6 and +7 (for example, $ReO_{(3+\delta)}$) [23]. Attribution of this peak to the formation of M–Re–O and M–Re alloy phases (M = Ni, Fe, Cr) was ruled out since these phases would give peaks at much lower binding energies.

While intermetallic Re phases have been used to provide unique active sites [12] and Re(IV) has been cited as a hydrogenation catalyst for carbon removal [24], neither of these are present in our system. Re(VI) and (VII) are also active hydrogenation catalysts, and account for 1/3 of the rhenium atoms in the catalyst layer. Therefore, we attribute the promotion of the DRM to the Re(VI) and Re(VII) oxide phases, in addition to the unique non-stoichiometric $ReO_{(3+\delta)}$ phase accounting for 62% of the rhenium atoms.

4. Conclusions

Through use of electrochemical alloying and thermal processing, we show that structured catalysts materials, such as the foams shown here, are viable candidates for methane reforming technologies, and can offer many advantages over their supported powder counterparts. Tuning of the foam's composition through rhenium alloying showed marked improvement in methane conversion at industrially relevant operating temperatures. Post-mortem analysis of the foams revealed no significant carbon accumulation, suggesting that Ni oxidation is the primary form of catalyst deactivation. Future research in this field will include tuning the redox properties of the foam to further resist Ni oxidation, and altering the synthesis to create foams with a larger specific surface area to enable the processing of methane at higher space velocities.

Acknowledgments

This work was supported in part by the Colton-Nadal Fund through RAMOT at Tel Aviv University. BAR was partially supported by an award from the Center for Nanoscience and Nanotechnology, Tel Aviv University and the J. William Fulbright Scholar program. The authors want to thank Prof. Sergey Cheskis for providing space for the catalyst testing setup, Dr. Larissa Burstein for collection of the XPS data, Dr. Yuri Rosenberg for collection of the XRD data, Dr. Vladamir Ezersky (BGU) and Prof. Amit Kohn (BGU) for TEM imaging, Dr. Atsmon Vakahy for FIB preparation of the TEM sample, Dr. Yoel Sasson (HUJI) and Hani Gnayem (HUJI) for BET measurements, Daria Zubenko and Moran Dahan for TPR measurements, and Tzippora Nusbaum for help with optimizing the electrochemical preparation. The authors also want to thank Mario Levishtein and Gil Hayoun for assisting with the construction of the experimental assemblies. All opinions expressed in this paper are solely those of the authors'.

Appendix A. Supplementary data

Supplementary data to this article can be found online at http://dx.doi.org/10.1016/j.catcom.2015.12.014.

References

[1] P. Ferreira-Aparicio, A. Guerrero-Ruiz, I. Rodrıguez-Ramos, Comparative study at low and medium reaction temperatures of syngas production by methane reforming with carbon dioxide over silica and alumina supported catalysts, Appl. Catal. A Gen. 170 (1998) 177.

[2] S. Wang, G. Lu, G.J. Millar, Carbon dioxide reforming of methane to produce synthesis gas over metal-supported catalysts: state of the art, Energy Fuel 10 (1996) 896.

[3] O. Muraza, A. Galadima, A review on coke management during dry reforming of methane, Int. J. Energy Res. (2015).

[4] C.E. Daza, J. Gallego, F. Mondragón, S. Moreno, R. Molina, High stability of Ce-promoted Ni/Mg–Al catalysts derived from hydrotalcites in dry reforming of methane, Fuel 89 (2010) 592.

[5] J. Guo, H. Lou, H. Zhao, D. Chai, X. Zheng, Dry reforming of methane over nickel catalysts supported on magnesium aluminate spinels, Appl. Catal. A Gen. 273 (2004) 75.

[6] D. San-José-Alonso, J. Juan-Juan, M. Illán-Gómez, M. Román-Martínez, Ni, Co and bimetallic Ni–Co catalysts for the dry reforming of methane, Appl. Catal. A Gen. 371 (2009) 54.

[7] Y. Matatov-Meytal, M. Sheintuch, Catalytic fibers and cloths, Appl. Catal. A Gen. 231 (2002) 1.

[8] F. Basile, P. Benito, P. Del Gallo, G. Fornasari, D. Gary, V. Rosetti, E. Scaventta, D. Tonelli, A. Vaccari, Highly conductive Ni steam reforming catalysts prepared by electrodeposition, Chem. Commun. (2008) 2917.

[9] X. Du, D. Zhang, L. Shi, R. Gao, J. Zhang, Coke-and sintering-resistant monolithic catalysts derived from in situ supported hydrotalcite-like films on Al wires for dry reforming of methane, Nanoscale 5 (2013) 2659.

[10] P.C. Bakala, E. Briot, Y. Millot, J.-Y. Piquemal, J.-M. Brégeault, Comparison of olefin metathesis by rhenium-containing γ-alumina or silica–aluminas and by some mesoporous analogues, J. Catal. 258 (2008) 61.

[11] K. Azzam, I. Babich, K. Seshan, L. Lefferts, Role of Re in Pt–Re/TiO_2 catalyst for water gas shift reaction: a mechanistic and kinetic study, Appl. Catal. B Environ. 80 (2008) 129.

[12] L. Wang, K. Murata, M. Inaba, Control of the product ratio of CO_2/(CO + CO_2) and inhibition of catalyst deactivation for steam reforming of gasoline to produce hydrogen, Appl. Catal. B Environ. 48 (2004) 243.

[13] P. Torniainen, X. Chu, L. Schmidt, Comparison of monolith-supported metals for the direct oxidation of methane to syngas, J. Catal. 146 (1994) 1.

[14] J. Claridge, M. Green, S. Tsang, Methane conversion to synthesis gas by partial oxidation and dry reforming over rhenium catalysts, Catal. Today 21 (1994) 455.

[15] R. Burch, The oxidation state of rhenium and its role in platinum rhenium reforming catalysts, Platin. Met. Rev. 22 (1978) 57.

[16] T. Nusbaum, B.A. Rosen, E. Gileadi, N. Eliaz, Effect of pulse on-time and peak current density on pulse plated Re–Ni alloys, J. Electrochem. Soc. 162 (2015) D250.

[17] S. Maria de Lima, J. Mansur Assaf, Ni–Fe catalysts based on perovskite-type oxides for dry reforming of methane to syngas, Catal. Lett. 108 (2006) 1–2.

[18] C.L. Briant, R.A. Mulford, Surface segregation in austenitic stainless steel, Metall. Trans. A 13 (1982) 745.

[19] S. Sokolov, E.V. Kondratenko, M.-M. Pohl, A. Barkschat, U. Rodemerck, Stable low-temperature dry reforming of methane over mesoporous La_2O_3–ZrO_2 supported Ni catalyst, Appl. Catal. B Environ. 113 (2012) 19.

[20] L. Guczi, G. Stefler, O. Geszti, I. Sajo, Z. Paszti, A. Tompos, Z. Schay, Methane dry reforming with CO_2: a study on surface carbon species, Appl. Catal. A Gen. 375 (2010) 236.

[21] M.K. Nikoo, N. Amin, Thermodynamic analysis of carbon dioxide reforming of methane in view of solid carbon formation, Fuel Process. Technol. 92 (2011) 678.

[22] A. Andreev, V. Idakiev, K. Kostov, M. Gabrovska, Water-gas shift reaction over nickel hydroxides, Catal. Lett. 31 (1995) 245.

[23] A. Naor, N. Eliaz, L. Burstein, E. Gileadi, Direct experimental support for the catalytic effect of iron-group metals on electrodeposition of rhenium, Electrochem. Solid-State Lett. 13 (2010) D91.

[24] M.F. Johnson, V. LeRoy, The state of rhenium in Pt/Re/alumina catalysts, J. Catal. 35 (1974) 434.